Theoretical Calculation of the Photodetachment Spectra of $XAuY^-$ (X, Y = Cl, Br, and I)

Sabyashachi Mishra*

Department of Chemistry, Technical University of Munich, D-85747, Garching, Germany

Received: May 14, 2007; In Final Form: July 8, 2007

The photodetachment spectra of the title molecules have been calculated, taking electron correlation and spin−orbit coupling into account and employing improved relativistic effective core potentials for gold and the halogen atoms. The calculated spectra have been compared with existing experimental spectra. The spin−orbit splitting of several degenerate electronic states has been calculated. The composition of the spin−orbit eigenstates are analyzed in terms of scalar relativistic electronic states. A comparison of the relative position of peaks in the calculated photodetachment spectra of the title molecules has been made.

Introduction

The chemistry of gold compounds has always been a hot topic due to the unique properties of gold, which are influenced by relativistic effects, and for its potential applications in material science, medicine, and catalysis. The multiple personalities of gold have been described in a recent review by Pyykkö, where a detailed account of the gold chemistry can be found.[1]

Recently, we assigned the photodetachment spectra (PDS) of Schröder et al.[2] for AuX_2^-, X = Cl, Br, and I, by taking spin−orbit (SO) coupling into account and employing improved relativistic effective core potentials (RECP) for gold and the halogen atoms.[3] We also emphasized the relevance of SO coupling in the spectroscopy of heavy elements by comparing our results with experiment[2] and with other scalar relativistic theoretical studies;[4] see ref 3.

While the symmetric gold dihalides (AuX_2^-) have received some attention,[2−8] the nonsymmetric gold dihalides ($XAuY^-$, X ≠ Y), to our knowledge, have remained unexplored.

In the present study, we have performed ab initio electronic structure calculations on $XAuY^-$ (X, Y = Cl, Br, and I), taking the SO coupling explicitly into account. Unlike the symmetric dihalides, the excited-state spectroscopy of the nonsymmetric dihalides cannot be properly described via single-reference correlation methods. Therefore, in contrast to our previous work,[3] where the coupled-cluster method was used, we have employed multireference methods to calculate the photodetachment spectra of the title molecules. In addition to a reassignment of the experimental PDS of the symmetric gold dihalides, our results lead to a theoretical prediction of the PDS of nonsymmetric gold dihalides, namely, $ClAuBr^-$, $ClAuI^-$, and $BrAuI^-$.

Ab Initio Calculations

The structural and electronic properties of $XAuY^-$ have been determined by using quantum chemical methods where the gold and halogen atoms are described by RECP. While the gold atom is described by two-component relativistic pseudopotentials (i.e., scalar relativistic and SO potentials) of the energy-consistent variety supplemented by an energy-optimized (12s12p9d3f2g)/[6s6p4d3f2g] valence basis set,[9] we have used one-component (i.e., SO averaged) semilocal energy-adjusted pseudopotentials for the halogen atoms.[10] The valence electrons of Br and I are described by basis sets of augmented quadruple-ζ quality, composed of optimized contracted s, p, d, f, and g functions,[10] whereas the valence shell of Cl is described by optimized contracted s and p functions of augmented quadruple-ζ quality.[11] The d, f, and g polarization functions are obtained from the augmented correlation-consistent polarized valence quadruple-ζ (aug-cc-pVQZ) basis set of Woon and Dunning.[12] A core polarization potential (CPP)[13] calculation for the halogen centers is performed during every calculation using the CPP parameters taken from ref 10.

The geometries of the XAuY anions have been optimized in their respective ground states by a scalar relativistic (neglecting SO effects) coupled-cluster calculation with singles and doubles and perturbative account of triple excitations (CCSD(T)). The calculations are performed in the largest Abelian point group of the corresponding systems, that is, D_{2h} for the symmetric (X = Y) and C_{2v} for the nonsymmetric (X ≠ Y) linear gold dihalides. The closed-shell anionic species possess an electronic ground state of $^1\Sigma_g^+$ symmetry with the following valence-shell electronic configuration: $1\sigma_g^2\,1\sigma_u^2\,1\pi_u^4\,2\sigma_g^2\,2\sigma_u^2\,3\sigma_g^2\,1\pi_g^4\,1\delta_g^4\,3\sigma_u^2\,2\pi_u^4\,4\sigma_g^2\,2\pi_g^4$ (g/u notation applies to the symmetric dihalides only). Detachment of one electron from the highest-occupied $2\pi_g$ molecular orbital of the anion gives rise to the $\tilde{X}^2\Pi_g$ ground state of the neutral species. We employ the multireference configuration interaction (MRCI) method, which uses state-averaged (over the lowest two $^2\Pi$, two $^2\Sigma^+$, and one $^2\Delta$ states) complete active space self-consistent field (SA-CASSCF) orbitals as the *N*-electron basis, for a scalar relativistic description of the lowest eight electronic states at the reference geometry of the anion. The active space involves all but 8 valence electrons, correlated in 14 orbitals.

The SO interaction was treated by the contracted SO configuration interaction method after the electron correlation step, diagonalizing the SO matrix in the space of all SO-free electronic states of interest.[14] The scalar relativistic orbitals obtained from the MRCI calculations are used to calculate the SO matrix elements. The SO matrix elements are computed using the SO pseudopotential cited above[9] for gold and SO pseudo-operators by Dolg,[11] adapted to the scalar RECP used for the halogen atoms.[10] All calculations have been performed using the MOLPRO program suite.[15]

* To whom correspondence should be addressed. E-mail: sabyashachi.mishra@ch.tum.de.

10.1021/jp0736645 CCC: $37.00
Published on Web 08/22/2007

TABLE 1: Optimized Bond Distances in Å at the CCSD(T) Level for $XAuY^-$

$XAuY^-$	X−Au	Au−Y
$AuCl_2^-$	2.2836	
$AuBr_2^-$	2.4086	
AuI_2^-	2.5754	
$ClAuBr^-$	2.2622	2.3984
$ClAuI^-$	2.2700	2.5564
$BrAuI^-$	2.4184	2.5647

TABLE 2: Scalar Relativistic Detachment Energies (in eV) from the $\tilde{X}\ ^1\Sigma^+$ State of $XAuY^-$ Computed by the MRCI/SA-CASSCF Method[a]

state	$AuCl_2$	state	$AuBr_2$	AuI_2
$\tilde{X}^2\Pi_g$	4.618	$\tilde{X}^2\Pi_g$	4.721	5.220
$\tilde{A}^2\Sigma_g^+$	4.863 (0.245)	$\tilde{A}^2\Sigma_g^+$	5.221 (0.500)	6.107 (0.887)
$\tilde{B}^2\Delta_g$	6.243 (1.625)	$\tilde{B}^2\Pi_u$	6.005 (1.284)	6.127 (0.907)
$\tilde{C}^2\Pi_u$	6.319 (1.701)	$\tilde{C}^2\Sigma_u^+$	6.236 (1.515)	6.332 (1.112)
$\tilde{D}^2\Sigma_u^+$	6.561 (1.943)	$\tilde{D}^2\Delta_g$	6.548 (1.827)	7.411 (2.191)
	ClAuBr		ClAuI	BrAuI
$\tilde{X}^2\Pi$	4.761	$\tilde{X}^2\Pi$	4.603	4.610
$\tilde{A}^2\Sigma^+$	5.165 (0.404)	$\tilde{A}^2\Sigma^+$	5.259 (0.656)	5.343 (0.733)
$\tilde{B}^2\Pi$	6.358 (1.597)	$\tilde{B}^2\Pi$	6.147 (1.544)	5.757 (1.147)
$\tilde{C}^2\Delta$	6.508 (1.747)	$\tilde{C}^2\Sigma^+$	6.170 (1.567)	5.918 (1.308)
$\tilde{D}^2\Sigma^+$	6.529 (1.768)	$\tilde{D}^2\Delta$	6.570 (1.967)	6.659 (2.049)

[a] Values in parentheses refer to the MRCI/SA-CASSCF results with the vertical detachment energy of the $\tilde{X}^2\Pi$ adjusted to zero.

Results and Discussion

The optimized geometries of the ground state of the symmetric and nonsymmetric XAuY anions are given in Table 1. For the comparison of calculated and experimental bond distances of AuX_2^- species, see ref 3. The Au−Cl bond length is found to be around 2.27 Å, whereas the Au−Br and Au−I bond distances are around 2.40 and 2.56 Å, respectively, for all of the species; see Table 1.

The vertical detachment energies of the lowest eight electronic states with respect to the electronic ground state of the anion ($\tilde{X}\ ^1\Sigma^+$) determined by performing MRCI/SA-CASSCF calculations are reported in Table 2. Since the energy spacing of the electronic states of the neutral XAuY matters, rather than the absolute values of the vertical detachment energies, we have also reported, in Table 2, the difference in vertical detachment energies of the excited states of the neutral XAuY with respect to its ground state. This allows a comparison of the relative positions of the scalar relativistic band heads of the PDS. The relative energies of the excited scalar relativistic electronic states of the neutral XAuY are plotted against their molecular weight in Figure 1. It is found that the electronic energies are a linear function of molecular mass, to a good approximation. While the energy difference of the (1) $^2\Sigma^+$ state and the (1) $^2\Delta$ state with respect to the (1) $^2\Pi$ state (the ground state) increases linearly with molecular mass, a reverse trend is observed for the (2) $^2\Sigma^+$ and (2) $^2\Pi$ states; see Figure 1. Several changes occur in the ordering of the electronic states when going from $AuCl_2$ to AuI_2. In particular, the $^2\Delta$ state, which lies high in the energy for AuI_2, is the second excited state in $AuCl_2$; see Figure 1. This electronic state was overlooked in our earlier work.[3] Although the $^2\Delta$ state will have a negligible effect on the observed spectroscopy of AuI_2 and, to some extent, $AuBr_2$, for $AuCl_2$, however, it is indispensable.

The calculated SO splittings in the two $^2\Pi$ states and the $^2\Delta$ state of XAuY are given in Table 3. The SO splitting of both of the $^2\Pi$ states increases, as expected, from $AuCl_2$ to AuI_2, with the exception of the small SO splitting of the (2) $^2\Pi$ state of $AuBr_2$. In Table 3, the numbers in parentheses are the SO splittings of the corresponding degenerate state when their coupling with neighboring states is neglected, that is, when they are assumed isolated. When compared with the true SO splitting, these numbers reveal the extent of interaction between different SO-free states via the SO coupling operator. In $AuCl_2$, the $\tilde{X}^2\Pi$ state interacts significantly with the $\tilde{A}^2\Sigma^+$ state via the SO interaction. The SO splitting of the former state decreases substantially (from its value in the isolated $^2\Pi$ state approximation) as a result of the repulsion of first two 1/2 states, which arise mainly from the $\tilde{A}^2\Sigma^+$ and $\tilde{X}\ ^2\Pi$ states; see Tables 3 and 4. This degree of interaction gets reduced for the heavier gold dihalides since the energy separation between the $\tilde{X}\ ^2\Pi$ and the $\tilde{A}^2\Sigma^+$ increases from $AuCl_2$ to AuI_2; see Figure 1. In AuI_2, for example, this mixing almost vanishes and so does the difference between the true SO splitting and the SO splitting from the isolated-state approximation; see Table 3. By comparing the true SO splitting and the SO splitting calculated with the inclusion of the SO contributions of only halide atoms (i.e., SO contributions from the Au atom are neglected), it is found that the halogen centers contribute about 80% of the total SO splitting of the (1) $^2\Pi$ state.

While the (1) $^2\Pi$ state arises from an orbital with antibonding overlap of gold and the halogen centers, the (2) $^2\Pi$ state emanates from the orbital centered primarily on the halogen centers. Therefore, the true SO splitting as well as the SO splitting obtained in the isolated-state approximation of the (2) $^2\Pi$ state, of which more than 98% are due to the halogen centers, increase from $AuCl_2$ to AuI_2. By comparing the SO splittings obtained from these two methods, it can be seen that the isolated-state approximation of the (2) $^2\Pi$ state gets poorer as one approaches heavier systems due to the increasing interaction of this state with the (2) $^2\Sigma^+$ state via the SO operator. Although the scalar relativistic energy difference between these two electronic states of all of the systems remains nearly the same, see Figure 1, for the heavier halides due to the large SO splitting in the (2) $^2\Pi$ state, the (2) $^2\Sigma^+$ state lies in between the 3/2 and 1/2 components of the (2) $^2\Pi$ state, and the repulsion between the low-lying $^2\Sigma_{1/2}^+$ state and the high-lying 1/2 component of the (2) $^2\Pi$ state increases the true SO splitting compared to the SO splitting in the isolated-state approximation.

The SO splitting of the $^2\Delta$ state remains nearly the same, that is, around 1.3 eV for all molecules. The calculated SO splitting in the $^2\Delta$ state of XAuY is quite similar to the atomic SO splitting of the 5d orbital of Au (1.5 eV), which is due to the fact that the $^2\Delta$ state originates from the molecular orbital localized on the central Au atom. The true SO splitting is only slightly different from the SO splitting obtained in the isolated-state approximation since the $^2\Delta$ state mixes only to a minor extent with the neighboring states via the SO operator.

Using the SO splittings given in Table 3 and the scalar relativistic MRCI energies given in Table 2, we have assigned the experimental PDS of the AuX_2^- and predicted the PDS of the nonsymmetric gold dihalides; see Tables 4 and 5, respectively. The calculated energy of the SO eigenstates is presented with respect to the energy of the (1) 3/2 state, which indicates the origin of the spectrum. The assignment of the spectra has been carried out by investigating the composition of the SO eigenstate in terms of scalar relativistic electronic states.

Similar to the previous study,[3] we assign the first two peaks (which are not completely resolved in the experimental spectrum of $AuCl_2^-$, see Figure 1a of ref 2) as the $3/2_g$ and $1/2_g$ SO components of the $\tilde{X}^2\Pi_g$ state, followed by the narrow and intense peak assigned as the $\tilde{A}^2\Sigma_{g,1/2}^+$ state; see Table 4. The

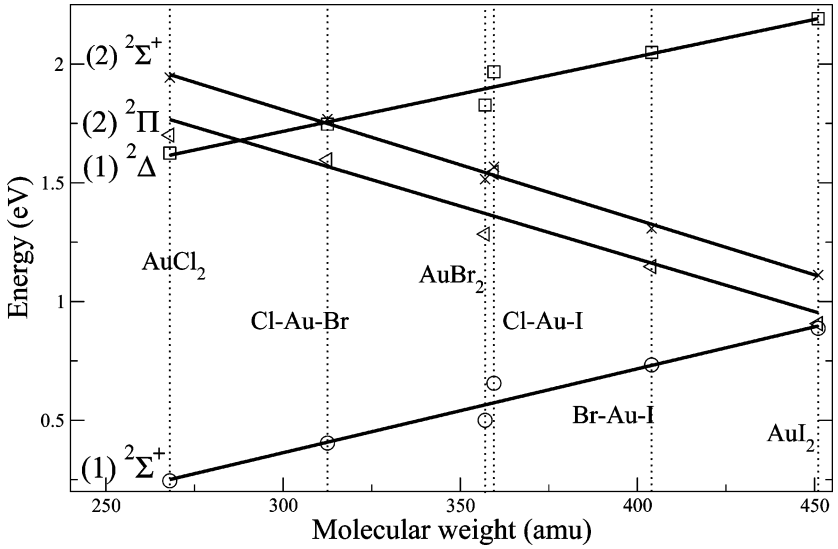

Figure 1. The relative energies of the scalar relativistic electronic states of the neutral XAuY with respect to the (1) $^2\Pi$ ground state, see Table 2, as a function of molecular weight. The calculated energies of the (1) $^2\Sigma^+$, (1) $^2\Delta$, (2) $^2\Pi$, and (2) $^2\Sigma^+$ states are shown by circles, squares, triangles, and crosses, respectively.

TABLE 3: SO Splitting (in eV) of the (1) $^2\Pi$, (2) $^2\Pi$, and (1) $^2\Delta$ States of XAuY, Computed in the Basis of the (1) and (2) $^2\Pi$, (1) $^2\Delta$, (1) and (2) $^2\Sigma^+$ SO-Free States[a]

	(1) $^2\Pi$	(2) $^2\Pi$	(1) $^2\Delta$
$AuCl_2$	0.0864 (0.4117)	0.0970 (0.0975)	1.3193 (1.2265)
ClAuBr	0.2273 (0.4590)	0.3199 (0.2728)	1.3666 (1.2485)
$AuBr_2$	0.3340 (0.4792)	0.1815 (0.3140)	1.3120 (1.2447)
ClAuI	0.4328 (0.5956)	0.6370 (0.4371)	1.3699 (1.2476)
BrAuI	0.5179 (0.5914)	0.7025 (0.4440)	1.3044 (1.2452)
AuI_2	0.6555 (0.6492)	0.9350 (0.5939)	1.2809 (1.2420)

[a] Values in parentheses refer to the results obtained when the concerned state is assumed to be isolated.

assignment of the next two peaks with very low intensity seen at higher energy differs from the assignment in ref 3. While the present multiconfigurational study reveals these two peaks as the lower SO components of the $\tilde{B}^2\Delta_g$ and the $\tilde{C}^2\Pi_u$, that is, the (1) $5/2_g$ and the (1) $3/2_u$ states, respectively, the results from ref 3, where the $^2\Delta_g$ state is not considered, assigned these two peaks as two SO components of the $^2\Pi_u$ state. An experimental probe at higher energy is hoped to detect the peaks due to the upper SO components of the $\tilde{B}^2\Delta_g$ and the $\tilde{C}^2\Pi_u$ states in the energy range given in Table 4. Similar conclusions can be made for $AuBr_2^-$ as well, where we assign the first two moderately intense peaks (Figure 1b of ref 2) as the two SO components of the $\tilde{X}^2\Pi_g$ state followed by the intense and narrow peak due to the $\tilde{A}^2\Sigma^+_{g,1/2}$ state. In contrast to the assignment in ref 3, the present study leads to the assignment of the next two well-separated and equi-intense peaks as due to the (1) $3/2_u$ and (1) $5/2_g$ states, respectively. These two peaks were assigned as the two SO components of the $^2\Pi_u$ state in ref 3. The assignment of the PDS of AuI_2^- remains unchanged from ref 3 since the $^2\Delta_g$ state, in this case, lies high in energy. The matching between the energies of the experimental photoelectron peaks and the energies obtained from present calculations is excellent in all three cases; see Table 4.

In Table 5, the calculated PDS of the nonsymmetric gold dihalides are presented. Similar to the AuX_2^-, the first three SO eigenstates in all three nonsymmetric gold dihalides correspond to the two SO components of the $\tilde{X}^2\Pi$ and the $\tilde{A}^2\Sigma^+$ states, respectively. The higher-energy SO eigenstates, however, are less ordered in different systems; see Table 5. Notice, for

TABLE 4: Assignment of Photoelectron Bands of Symmetric Gold Dihalides (AuX_2) and Composition of the SO Eigenstates in Terms of SO-Free States; All Energies in eV

SO state	calcd	exptl	composition (weight in %)
		$AuCl_2$	
(1) $3/2_g$	0.00	0.00	$\tilde{X}^2\Pi_g$ (95); $\tilde{B}^2\Delta_g$ (5)
(1) $1/2_g$	0.09	0.20	$\tilde{X}^2\Pi_g$ (55); $\tilde{A}^2\Sigma^+_g$ (45)
(2) $1/2_g$	0.96	0.99	$\tilde{X}^2\Pi_g$ (45); $\tilde{A}^2\Sigma^+_g$ (55)
(1) $5/2_g$	1.31	1.44	$\tilde{B}^2\Delta_g$ (100)
(1) $3/2_u$	1.95	1.57	$\tilde{C}^2\Pi_u$ (100)
(1) $1/2_u$	2.05		$\tilde{C}^2\Pi_u$ (100)
(2) $1/2_u$	2.24		$\tilde{D}^2\Sigma^+_u$ (100)
(2) $3/2_g$	2.63		$\tilde{X}^2\Pi_g$ (5); $\tilde{B}^2\Delta_g$ (95)
		$AuBr_2$	
(1) $3/2_g$	0.00	0.00	$\tilde{X}^2\Pi_g$ (95); $\tilde{D}^2\Delta_g$ (5)
(1) $1/2_g$	0.34	0.35	$\tilde{X}^2\Pi_g$ (70); $\tilde{A}^2\Sigma^+_g$ (30)
(2) $1/2_g$	1.02	1.03	$\tilde{X}^2\Pi_g$ (30); $\tilde{A}^2\Sigma^+_g$ (70)
(1) $3/2_u$	1.44	1.26	$\tilde{B}^2\Pi_u$ (100)
(1) $5/2_g$	1.51	1.50	$\tilde{D}^2\Delta_g$ (100)
(1) $1/2_u$	1.62		$\tilde{B}^2\Pi_u$ (60); $\tilde{C}^2\Sigma^+_u$ (40)
(2) $1/2_u$	1.95		$\tilde{B}^2\Pi_u$ (40); $\tilde{C}\Sigma^{2+}_u$ (60)
(2) $3/2_g$	2.82		$\tilde{X}^2\Pi_g$ (5); $\tilde{D}^2\Delta_g$ (95)
		AuI_2	
(1) $3/2_g$	0.00	0.00	$\tilde{X}^2\Pi_g$ (100)
(1) $1/2_g$	0.66	0.62	$\tilde{X}^2\Pi_g$ (100)
(1) $3/2_u$	0.97	0.90	$\tilde{B}^2\Pi_u$ (100)
(1) $1/2_u$	1.14	1.13	$\tilde{B}^2\Pi_u$ (45); $\tilde{C}^2\Sigma^+_u$ (55)
(2) $1/2_g$	1.28	1.44	$\tilde{A}^2\Sigma^+_g$ (100)
(2) $1/2_u$	1.91	1.98	$\tilde{B}^2\Pi_u$ (55); $\tilde{C}^2\Sigma^+_u$ (45)
(1) $5/2_g$	1.93		$\tilde{D}^2\Delta_g$ (100)
(2) $3/2_g$	3.21		$\tilde{D}^2\Delta_g$ (100)

the symmetric dihalides, where the calculations are performed under D_{2h} point group, the $^2\Delta$ state with gerade symmetry mixes, to a small extent, with the (1) $^2\Pi$ state but not with the (2) $^2\Pi$ state since the latter has ungerade symmetry. In the case of the nonsymmetric dihalides, on the other hand, where the g/u symmetry is absent, the (1) $^2\Delta$ state mixes with the close-lying (2) $^2\Pi$ state rather than with the far-lying (1) $^2\Pi$ state; see Tables 4 and 5.

The calculated SO eigenenergies of all six systems studied here are plotted against their molecular weights in Figure 2. The energies of the SO eigenstates, like the scalar relativistic

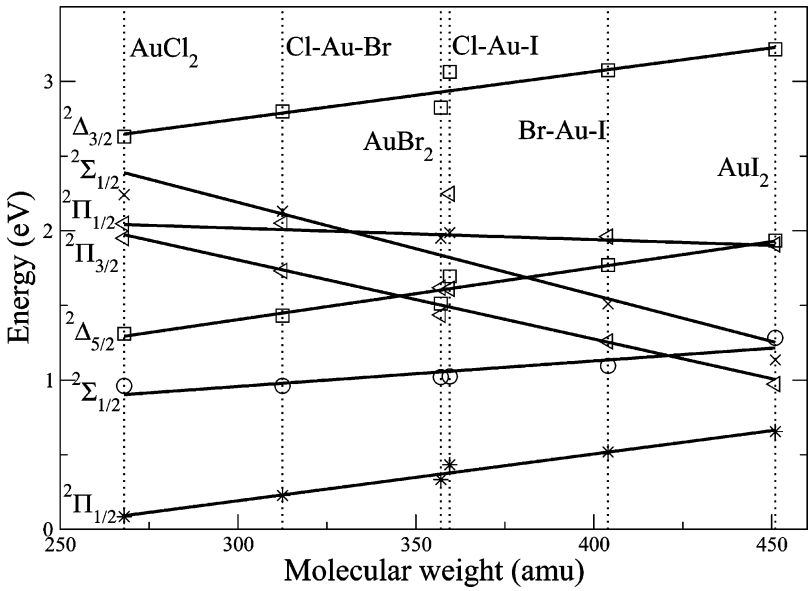

Figure 2. The relative energies of the SO eigenstates of the neutral XAuY with respect to the (1) $^2\Pi_{3/2}$ state as a function of molecular weight. The calculated energies of the SO components of the (1) $^2\Pi$, (1) $^2\Sigma^+$, (1) $^2\Delta$, (2) $^2\Pi$, and (2) $^2\Sigma^+$ states are shown by stars, circles, squares, triangles, and crosses, respectively. Although the SO eigenstates are a mixture of the SO-free states and the orbital angular momentum quantum number, Λ (Σ, Π, etc.) is no longer a good quantum number, and the states are labeled with the Λ value of the largest contributing SO-free electronic state; see Tables 4 and 5.

TABLE 5: Theoretical Prediction of the Photoelectron Bands of Nonsymmetric Gold Dihalides (XAuY, X ≠ Y) and Composition of the SO Eigenstates in Terms of SO-Free States; All Energies in eV

SO state	energy	composition (weight in %)
		ClAuBr
(1) 3/2	0.00	$\tilde{X}^2\Pi$ (97); $\tilde{C}^2\Delta$ (3)
(1) 1/2	0.23	$\tilde{X}^2\Pi$ (60); $\tilde{A}^2\Sigma^+$ (40)
(2) 1/2	0.96	$\tilde{X}^2\Pi$ (40); $\tilde{A}^2\Sigma^+$ (60)
(1) 5/2	1.43	$\tilde{C}^2\Delta$ (100)
(2) 3/2	1.73	$\tilde{B}^2\Pi$ (96); $\tilde{C}^2\Delta$ (4)
(3) 1/2	2.05	$\tilde{B}^2\Pi$ (60); $\tilde{D}^2\Sigma^+$ (40)
(4) 1/2	2.13	$\tilde{B}^2\Pi$ (40); $\tilde{D}^2\Sigma^+$ (60)
(3) 3/2	2.80	$\tilde{X}^2\Pi$ (3); $\tilde{B}^2\Pi$ (4); $\tilde{C}^2\Delta$ (93)
		ClAuI
(1) 3/2	0.00	$\tilde{X}^2\Pi$ (100)
(1) 1/2	0.43	$\tilde{X}^2\Pi$ (76); $\tilde{A}^2\Sigma^+$ (20); $\tilde{C}^2\Sigma^+$ (4)
(2) 1/2	1.02	$\tilde{X}^2\Pi$ (18); $\tilde{A}^2\Sigma^+$ (72); $\tilde{B}^2\Pi$ (6); $\tilde{C}^2\Sigma^+$ (4)
(2) 3/2	1.61	$\tilde{B}^2\Pi$ (95); $\tilde{D}^2\Delta$ (5)
(1) 5/2	1.70	$\tilde{D}^2\Delta$ (100)
(3) 1/2	1.99	$\tilde{X}^2\Pi$ (6); $\tilde{A}^2\Sigma^+$ (3); $\tilde{B}^2\Pi$ (13); $\tilde{C}^2\Sigma^+$ (78)
(4) 1/2	2.25	$\tilde{A}^2\Sigma^+$ (5); $\tilde{B}^2\Pi$ (81); $\tilde{C}^2\Sigma^+$ (14)
(3) 3/2	3.06	$\tilde{B}^2\Pi$ (5); $\tilde{D}^2\Delta$ (95)
		BrAuI
(1) 3/2	0.00	$\tilde{X}^2\Pi$ (100)
(1) 1/2	0.52	$\tilde{X}^2\Pi$ (85); $\tilde{A}^2\Sigma^+$ (15)
(2) 1/2	1.10	$\tilde{X}^2\Pi$ (10); $\tilde{A}^2\Sigma^+$ (75); $\tilde{B}^2\Pi$ (10); $\tilde{C}^2\Sigma^+$ (5)
(2) 3/2	1.26	$\tilde{B}^2\Pi$ (100)
(3) 1/2	1.51	$\tilde{X}^2\Pi$ (5); $\tilde{A}^2\Sigma^+$ (10); $\tilde{B}^2\Pi$ (35); $\tilde{C}^2\Sigma^+$ (50)
(1) 5/2	1.77	$\tilde{D}^2\Delta$ (100)
(4) 1/2	1.96	$\tilde{B}^2\Pi$ (55); $\tilde{C}^2\Sigma^+$ (45)
(3) 3/2	3.07	$\tilde{D}^2\Delta$ (100)

energies in Figure 1, change linearly with the molecular mass. Figure 2 provides a graphical presentation of the change in SO splitting of the (1) and (2) $^2\Pi$ and (1) $^2\Delta$ states as one goes from $AuCl_2$ to AuI_2. As discussed earlier, the SO splitting of the $^2\Delta$ state remains unchanged, whereas that of the (1) and (2) $^2\Pi$ states increases with increasing relativistic effects; see Figure 2. There are several instances of reordering of energy levels as a function of the molecular weight (or relativistic effects).

Conclusions

We have determined the geometries of anionic XAuY (X, Y = Cl, Br, and I) at the CCSD(T) level, employing an improved RECP for Au and the halogens. The SO-free vertical detachment energies of the ground as well as of the excited states of the neutral species have been determined using the MRCI method, where eight electronic states are averaged, via a SA-CASSCF calculation, to generate the *N*-electron basis. We have also determined SO coupling parameters of these complexes by calculating the matrix elements of the SO operator over the SO-free CI vectors. The SO splittings in the degenerate states have been compared for different species.

We have not only reported a revised assignment of the experimentally recorded PDS of symmetric gold dihalides, that is, when X = Y, but we also have provided a theoretical prediction of PDS of the nonsymmetric gold dihalides (X ≠ Y). For symmetric gold dihalides, we have compared the present assignment with the previous assignment where the presence of the excited $^2\Delta_g$ state was overlooked.[3] While this state has a negligible effect on the observed spectroscopy of AuI_2, for $AuBr_2$ and $AuCl_2$, the inclusion of this state is found to be necessary. Interestingly, the energy of the SO eigenstates of these molecules are found to change linearly with increasing molecular weight. It is hoped that this theoretical study will stimulate the recording of PDS of both symmetric as well as nonsymmetric gold dihalides over an extended range of photodetachment energies.

Acknowledgment. The author is grateful to Professor Wolfgang Domcke and Dr. Valérie Vallet for useful comments on the manuscript. This paper is dedicated to Professor Wolfgang Domcke, who introduced the author to this field of study, on the occasion of his 60th birthday.

References and Notes

(1) Pyykkö, P. *Angew. Chem., Int. Ed.* **2004**, *43*, 4412.
(2) Schröder, D.; Brown, R.; Schwerdtfeger, P.; Wang, X. B.; Yang, X.; Wang, L.; Schwarz, H. *Angew. Chem., Int. Ed.* **2003**, *42*, 311.
(3) Mishra, S.; Vallet, V.; Domcke, W. *ChemPhysChem* **2006**, *7*, 723.

(4) Dai, B.; Yang, J. *Chem. Phys. Lett.* **2005**, *379*, 512.
(5) Schwerdtfeger, P.; Boyd, P. D. W.; Burrell, A. K.; Robinson, W. T.; Taylor, M. J. *Inorg. Chem.* **1990**, *29*, 3593.
(6) Schwerdtfeger, P.; McFeaters, J. S.; Stephens, R. L.; Liddell, M. J.; Dolg, M.; Hess, B. A. *Chem. Phys. Lett.* **1994**, *218*, 362.
(7) Schwerdtfeger, P.; McFeaters, J. S.; Liddell, M. J.; Hrušák, J.; Schwarz, H. *J. Chem. Phys.* **1995**, *103*, 245.
(8) Seth, M.; Cooke, F.; Schwerdtfeger, P.; Heully, J. L.; Pelissier, M. *J. Chem. Phys.* **1998**, *109*, 3935.
(9) Figgen, D.; Rauhut, G.; Dolg, M.; Stoll, H. *Chem. Phys.* **2005**, *311*, 227.
(10) Bergner, A.; Dolg, M.; Kuechle, W.; Stoll, H.; Preuss, H. *Mol. Phys.* **1993**, *80*, 1431.
(11) Dolg, M. Ph.D. Thesis, University of Stuttgart, Germany, 1989.
(12) Woon, D. E.; Dunning, T. H., Jr. *Chem. Phys.* **1993**, *98*, 1358.
(13) Dolg, M. In *Relativistic Electronic Structure Theory, Part 1. Fundamentals*; Schwerdtfeger, P., Ed.; Elsevier: Amsterdam, The Netherlands, 2004.
(14) Berning, A.; Schweizer, M.; Werner, H. J.; Knowles, P. J.; Palmieri, P. *Mol. Phys.* **2000**, *98*, 1823.
(15) Molpro 2002.6, a package of ab initio programs; see http://www.molpro.net.